AMERICAN SOCIETY FOR MICROBIOLOGY | mSphere

Check for updates

| Editor's Pick | Microbial Pathogenesis | Research Article

Time-resolved multi-omics reveals diverse metabolic strategies of *Salmonella* during diet-induced inflammation

Katherine Kokkinias,[1] Anice Sabag-Daigle,[2] Yongseok Kim,[3] Ikaia Leleiwi,[4] Michael Shaffer,[5] Richard Kevorkian,[5] Rebecca A. Daly,[5] Vicki H. Wysocki,[3] Mikayla A. Borton,[5] Brian M. M. Ahmer,[2] Kelly C. Wrighton[1,4,5]

AUTHOR AFFILIATIONS See affiliation list on p. 15.

ABSTRACT With a rise in antibiotic resistance and chronic infection, the metabolic response of *Salmonella enterica* serovar Typhimurium to various dietary conditions over time remains an understudied avenue for novel, targeted therapeutics. Elucidating how enteric pathogens respond to dietary variation not only helps us decipher the metabolic strategies leveraged for expansion but also assists in proposing targets for therapeutic interventions. In this study, we use a multi-omics approach to identify the metabolic response of *Salmonella enterica* serovar Typhimurium in mice on both a fibrous diet and high-fat diet over time. When comparing *Salmonella* gene expression between diets, we found a preferential use of respiratory electron acceptors consistent with increased inflammation in high-fat diet mice. Looking at the high-fat diet over the course of infection, we noticed heterogeneity in samples based on *Salmonella* ribosomal activity, which is separated into three infection phases: early, peak, and late. We identified key respiratory, carbon, and pathogenesis gene expressions descriptive of each phase. Surprisingly, we identified genes associated with host cell entry expressed throughout infection, suggesting subpopulations of *Salmonella* or stress-induced dysregulation. Collectively, these results highlight not only the sensitivity of *Salmonella* to its environment but also identify phase-specific genes that may be used as therapeutic targets to reduce infection.

IMPORTANCE Identifying novel therapeutic strategies for *Salmonella* infection that occur in relevant diets and over time is needed with the rise of antibiotic resistance and global shifts toward Western diets that are high in fat and low in fiber. Mice on a high-fat diet are more inflamed compared to those on a fibrous diet, creating an environment that results in more favorable energy generation for *Salmonella*. We observed differential gene expression across infection phases in mice over time on a high-fat diet. Together, these findings reveal the metabolic tuning of *Salmonella* to dietary and temporal perturbations. Research like this, which explores the dimensions of pathogen metabolic plasticity, can pave the way for rationally designed strategies to control disease.

KEYWORDS RNA-seq, time series, respiration, microbial metabolism, pathogenesis, CBA/J mice

Salmonella enterica serovar Typhimurium (*Salmonella*) is a leading cause of gastrointestinal disease worldwide, posing serious public health risks due to increasing antibiotic resistance (1, 2). One challenge of controlling this pathogen is its broad metabolic capacity and adaptability to its environment. Recent studies have demonstrated that *Salmonella* infection can be modified with a robust microbiome and through diet manipulation (3–7). However, mechanisms explaining these diet-based phenomena remain understudied. In this study, we address this knowledge gap by leveraging

Editor Sarah E. F. D'Orazio, University of Kentucky College of Medicine, Lexington, Kentucky, USA

Address correspondence to Kelly C. Wrighton, kelly.wrighton@colostate.edu.

The authors declare no conflict of interest.

See the funding table on p. 16.

Received 24 June 2024
Accepted 22 July 2024
Published 10 September 2024

deeply sequenced, time-series transcriptomics to reveal the metabolism of *Salmonella* throughout infection.

As a facultative anerobe, *Salmonella* outcompetes the native microbiota through stimulation of the host's inflammatory response and numerous virulence factors (8–11). In addition to oxygen diffusion into the gut lumen, the subsequent inflammatory response results in the generation of reactive oxygen and nitrogen species, which produce respiratory electron acceptors such as nitrate, nitrite, dimethyl sulfoxide (DMSO), trimethylamine N-oxide (TMAO), fumarate, tetrathionate, and thiosulfate (12–18). Furthermore, various carbon sources become available to *Salmonella* with inflammation. *Salmonella* can utilize host and microbial metabolic end products, such as lactate and ethanolamine, as well as microbial-derived succinate, and more energetically favorable carbon sources (18–24). Most studies evaluating *Salmonella* substrate and electron acceptor use focus on a single compound. Moreover, these studies often do not track metabolism under different dietary conditions or over time, primarily focusing on late-stage infection processes.

Diet is a critical driver of gut microbiomes, influencing the gut metabolic landscape and microbial membership, which can alter colonization resistance against *Salmonella* (25–28). For example, high-fat diets (HFDs) result in increased inflammation and host susceptibility to infection (29–31). Furthermore, prior research demonstrated that pretreatment with a high-fat, low-fiber, Western diet was sufficient to destroy pathogen colonization resistance, resulting in increased susceptibility to *Salmonella* (3). Given the expansion of the Western diet globally (32), studying *Salmonella* pathogenesis and physiology in more realistic diet backgrounds is needed.

Changes in the microbial membership, chemical landscape of the gut, and host response are dynamic factors exploited by pathogens like *Salmonella* (9, 11, 13). Yet, time-series studies are limited in this field. In this study, we analyze *Salmonella* gene expression from CBA mice fed with fibrous or high-fat diets over time. By pairing 16S rRNA sequencing, metatranscriptomic sequencing, lipocalin-2 analysis, and both targeted and untargeted metabolomics, we revealed known and previously unrecognized metabolic strategies that distinguish early, peak, and late infection phases. These data emphasize the importance of the environmental context to *Salmonella* metabolism and demonstrate preferential expression of metabolic and pathogenic pathways by diet and infection phase. These key pathways could be targeted to abate enteric infection.

RESULTS AND DISCUSSION

High-fat diet increases inflammation and *Salmonella* respiratory electron acceptor utilization

Using fecal samples, we assessed the role of diet on *Salmonella* infection by comparing the effects of a fibrous chow diet (Chow) or a high-fat diet (HFD) on *Salmonella* relative abundance, *Salmonella* gene expression, and mouse inflammation (Fig. 1A). First, we used 16S rRNA amplicon sequencing (16S) to screen the relative abundance of *Salmonella* per mouse and compared microbial community metrics between the two diets. We assessed nine *Salmonella*-infected mice on days 8 (HFD) and 11 (Chow), along with paired pre-infection samples from the same mice (n = 18). HFD mice were euthanized on day 8 due to severe disease represented by diarrhea, animal behavior, and animal lethargy, following the Ohio State University Institutional Animal Care and Use Committee (IACUC; OSU 2009A0035) protocols, while Chow mice were euthanized on day 16. Days 8 (HFD) and 11 (Chow) were chosen as late-infection samples based on peak *Salmonella* relative abundance (33) and sample availability (Fig. S2; Data Set S1).

All selected mice, regardless of diet, were classified as high responders with *Salmonella* relative abundance >25% (Fig. 1B) (9, 33). The HFD (97%) had a slightly higher average *Salmonella* relative abundance compared to the Chow (82%). Despite these slight differences, there was no significant difference in the microbial diversity between the two treatments at late infection (ANOVA, $P = 0.386$ and $P = 0.133$) (Fig. S1). Regardless of the dietary treatment, the paired pre-infection samples exhibited decreased microbial

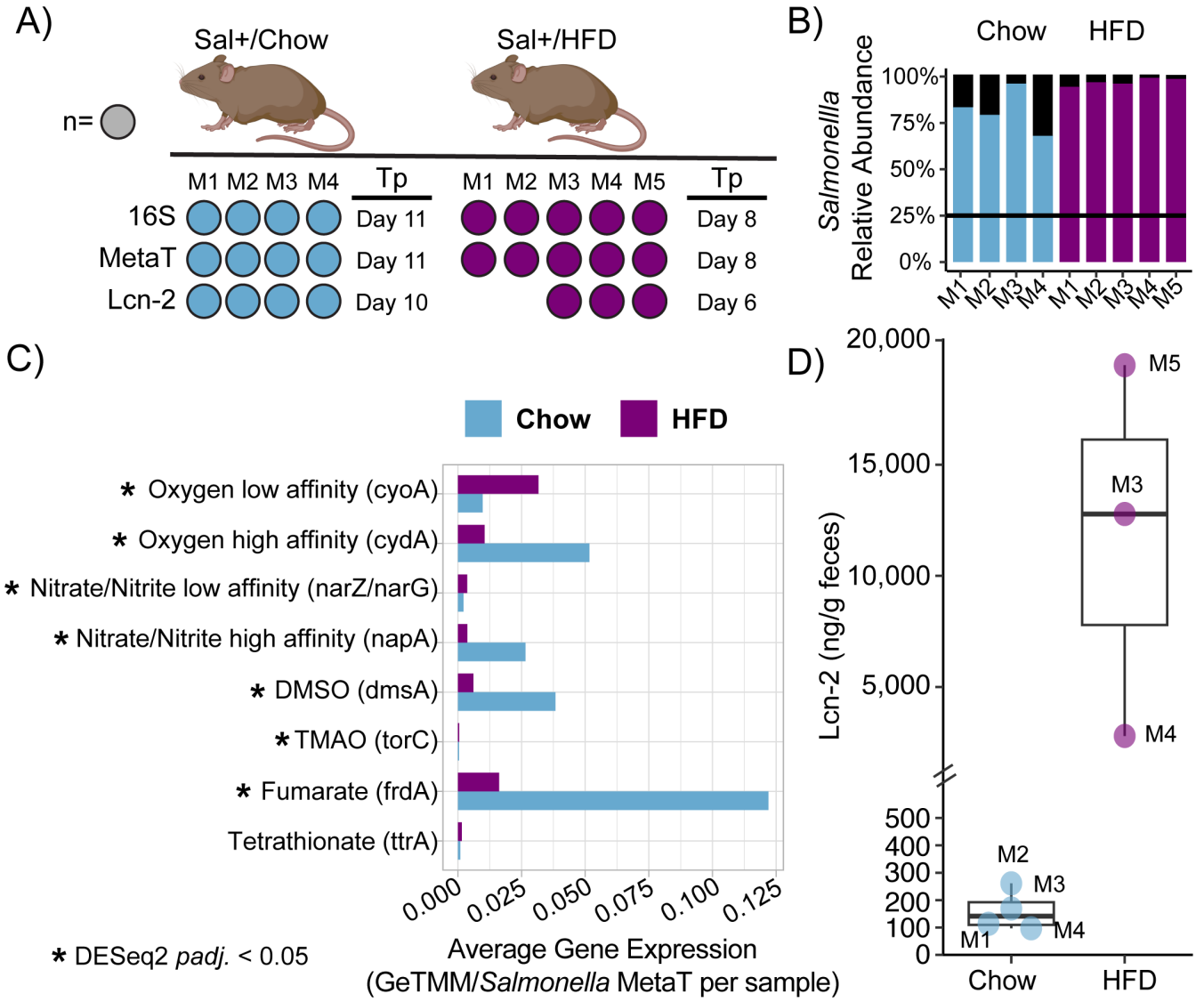

FIG 1 Increased inflammation and use of respiratory electron acceptors when comparing HFD and Chow mice. (A) Experimental design figure describes the number of mice, the dietary treatment, and types of analyses that were conducted. A filled circle denotes that the assay was performed for that specific mouse (mice 1–5). 16S rRNA amplicon sequencing (16S), metatranscriptomics (MetaT), and lipocalin-2 ELISA assays (Lcn-2) were conducted on fecal samples from mice fed with either chow diet (Chow, blue) or high-fat diet (HFD, purple) with the timepoint (Tp) indicated. (B) Stacked bar chart shows *Salmonella* abundance (colored blue or purple based on diet) for each mouse relative to the rest of the microbial community (denoted by black bars), as determined from 16S rRNA amplicon sequencing. The black line denotes samples that are high responders (25% *Salmonella* relative abundance). (C) The bar chart shows average *Salmonella* gene expression as gene length-corrected trimmed mean of M-values (GeTMM) for key respiratory electron acceptors between Chow and HFD mice. The asterisk indicates that the gene was significantly expressed between dietary regimes by DESeq2 (adjusted *P*-value < 0.05). (D) Box plot shows the median and Q1/Q3 ± 1.5 interquartile range of concentrations of lipocalin-2 (ng/g), as a measure of inflammation, from fecal samples for Chow and HFD mice.

richness and Shannon's diversity compared to their respective post-infection samples. Consistent with reports from others (3, 34), Chow pre-infection samples had significantly higher microbial diversity than HFD pre-infection samples (ANOVA, $P < 0.001$ and $P = 0.008$, respectively). This finding suggests that diet disrupts the microbiome, potentially impacting *Salmonella* physiology.

Along with *Salmonella* relative abundance, we measured lipocalin (Lcn-2) concentrations, which is a host-derived protein indicating inflammatory status (35). Lcn-2 concentrations (ng/g of feces) illustrated a significant increase in inflammation in HFD mice compared to Chow mice (Fig. 1D) (ANOVA, $P < 0.001$). Together, the 16S and lipocalin analyses illustrate that while diet alone can reduce the microbial diversity, the

presence of *Salmonella* results in more pronounced inflammation in HFD mice during late infection.

To ensure higher fidelity of our experimental results and address potential strain heterogeneity that may have developed during laboratory maintenance of *Salmonella enterica* serovar Typhimurium strain 14028 (36–39), we constructed a draft genome for this *Salmonella* isolate. This pangenome was derived from a combination of short and long read sequences (see Materials and Methods). This strain-resolved genome shared 4,597 called genes with 99.99% average nucleotide identity to the previously published *Salmonella* ATCC genome (SAMN08777876). Our metatranscriptomic sampling averaged 27.19 Gbp of sequences per sample, generating 1,363,165,050 reads. The internally derived genome was used to map metatranscriptomic sequences from nine fecal samples (Chow = 4; HFD = 5) and resulted in consistent read mapping regardless of diet.

Prior reports have suggested that inflammation increases electron acceptor availability (8, 11, 12, 20), which favors *Salmonella* growth during infection. As such, we hypothesized that we would see increased respiratory electron acceptor expression concurrent with increased inflammation in the HFD. *Salmonella* gene expression revealed that oxygen (*cyoA* and *cydA*), nitrate and nitrite (*narZ*/*narG* and *napA*), DMSO (*dmsA*), TMAO (*torC*), and fumarate (*frdA*) utilization genes were differentially expressed in either the HFD or Chow diet (Fig. 1C; Data Set S2). A variety of anoxic *Salmonella* respiration genes were differentially expressed in the Chow diet. Tetrathionate reduction (*ttrA*), while detected, did not show significant expression differences across diet treatments.

Additionally, when *Salmonella* encodes multiple genes for utilizing an electron acceptor, like oxygen and nitrogen, we observed increased expression of genes that function optimally at higher substrate concentrations and are more energetically favorable. Specifically, in the HFD, *Salmonella* preferentially expressed the low-affinity oxygen (*cyoA*) and nitrate (*narZ/narG*) utilization genes, compared to the less inflamed Chow treatment, where *Salmonella* activated the high-affinity oxygen (*cydA*) and nitrate (*napA*) utilization genes (40–44). Collectively, our results indicate that *Salmonella* gene expression responds to HFD-induced inflammation and suggests that *Salmonella* can finely tune its energetic strategy to local chemical conditions. These findings warrant further investigation and quantification of respiratory electron acceptors *in vivo* using non-invasive methods (45, 46).

Salmonella respiration is structured by the infection phase in HFD-fed mice

We next observed the progression of *Salmonella* metabolism throughout infection. We collected fecal samples from five HFD mice 1, 2, 3, and 6 days before *Salmonella* inoculation and continued daily sampling after inoculation until euthanization (day 8). Fecal samples were processed for 16S rRNA amplicon sequencing (16S), metatranscriptomics (metaT), lipocalin-2 ELISA assays (Lcn-2), targeted short-chain fatty acid (SCFA) metabolomics, and untargeted metabolomics (LC-MS) (Fig. 2A). Amplicon sequencing was used to profile *Salmonella* relative abundance across all 60 samples, guiding metatranscriptomic sample selection (Data Set S1). We collected metatranscriptomes during infection days 1, 3, 5, and 8, as well as day −1, analyzing 5,339,114,584 reads from 25 samples, with an average depth of 32.25 Gbp per sample (Data Set S2).

Time-series amplicon data showed that all HFD mice became high responders by day 5, but we note that there was heterogeneity among mice in the timing of peak *Salmonella* relative abundance and *Salmonella* cecal colony-forming unit (CFU) values (Fig. S3). Consequently, we used expression of the single-copy S3 ribosomal protein (*rpsC*) from *Salmonella* to group samples by the infection phase relative to each mouse over time (Fig. 2B). As shown in Fig. 2B, peak expression of *Salmonella* varied over time and between mice. Using the relative increase of S3 gene expression per mouse, we clustered the samples into three infection phases: early (nine samples), peak (five samples), and late (six samples) (Fig. 2C) (see Materials and Methods).

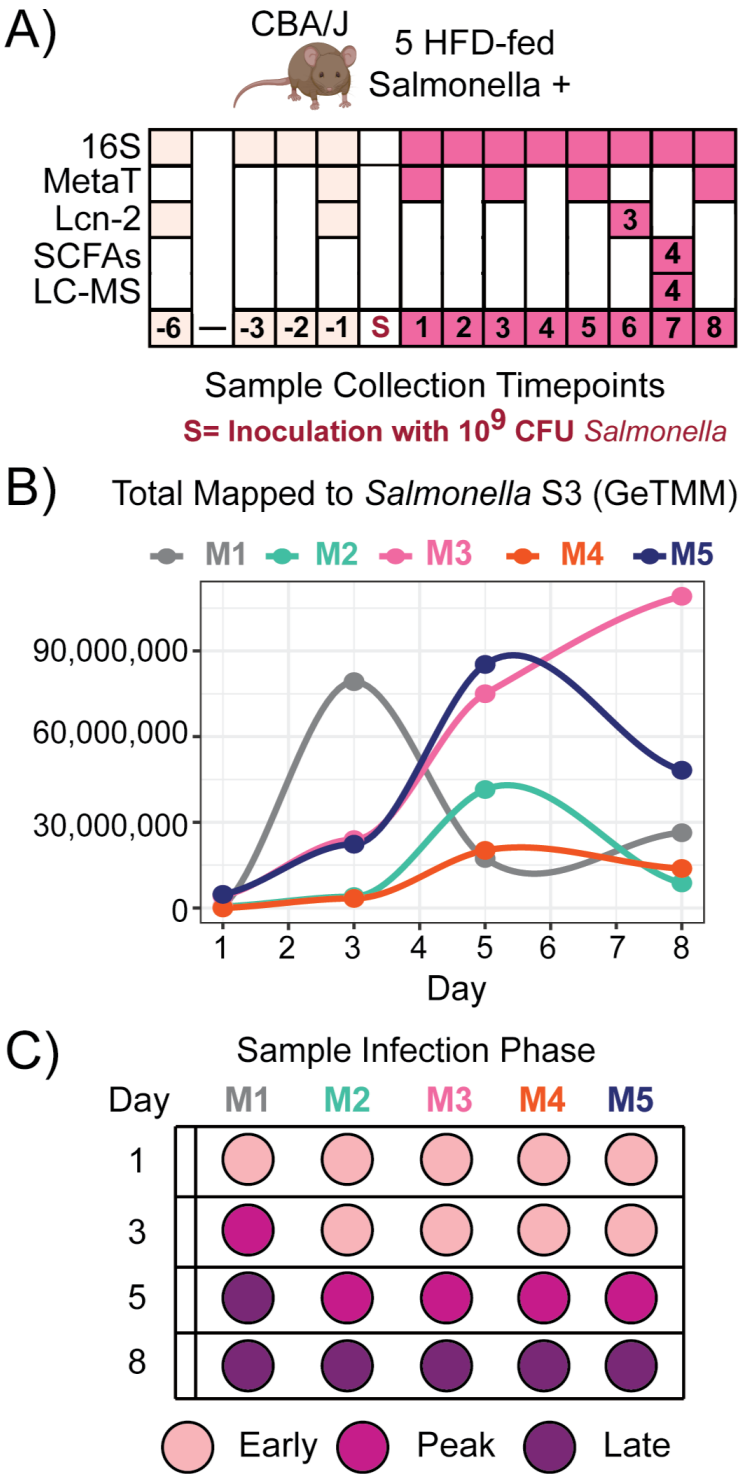

FIG 2 *Salmonella* infection heterogeneity over time. (A) High-fat diet (HFD) experimental design of five mice describes the types of analyses that were conducted on fecal samples over time. 16S rRNA amplicon sequencing (16S), metatranscriptomics (MetaT), lipocalin-2 ELISA assay (Lcn-2), targeted short-chain fatty acid (SCFA) metabolomics, and untargeted metabolomics (LC-MS) were conducted prior to infection (light pink) and after inoculation with 10^9 CFU *Salmonella* (dark pink). Analyses were performed on fecal samples from all five mice, unless noted otherwise by numbers within colored boxes. (B) The line plot shows normalized single-copy marker gene expression (GeTMM) of the *Salmonella* S3 ribosomal protein per mouse over time. (C) Given the heterogeneity of *Salmonella* gene expression over time, samples were grouped into infection phase (early: light pink, peak: dark pink, and late: purple).

Using our study metatranscriptomics data and the sample grouping described previously, we compared the expression of oxygen (*cyoABCDE* and *cydAB*), nitrate (*narGVZ*), TMAO (*torA*), tetrathionate (*ttrS*), thiosulfate (*phsABC*), and hydrogen (*hybC*) utilization genes (Fig. 3). These genes were differentially expressed between the infection phases according to DESeq2 or clustering by GeTMM normalization (Data Set S2). Our findings revealed selective utilization of respiratory electron acceptors during infection phases in HFD-fed mice (Fig. 3). Early- and late-infection phases exhibited increased expression of anerobic respiration genes (*narGVZ* and *phsABC*), while the peak infection phase showed increased expression of aerobic respiration genes (*cyoABCDE* and *cydAB*). Of these respiratory complexes, only the catalytic subunits for tetrathionate showed no differential temporal signal; however, the sensor for tetrathionate (*ttrS*) was distinctive in the early samples. Consistent with prior research, this respiratory capacity provides *Salmonella* a competitive advantage against obligate fermentative microorganisms prevalent in the pre-infection gut (8, 33, 47–49).

Our findings indicate differential electron acceptor use along the infection gradient in a HFD background. It was not surprising to see oxygen use, the most energetically favorable electron acceptor, at peak infection when *Salmonella* ribosomal protein expression was also highest, as the lumen becomes more oxygenated in response to *Salmonella* (13). Interestingly, genes encoding anerobic respiration were more highly

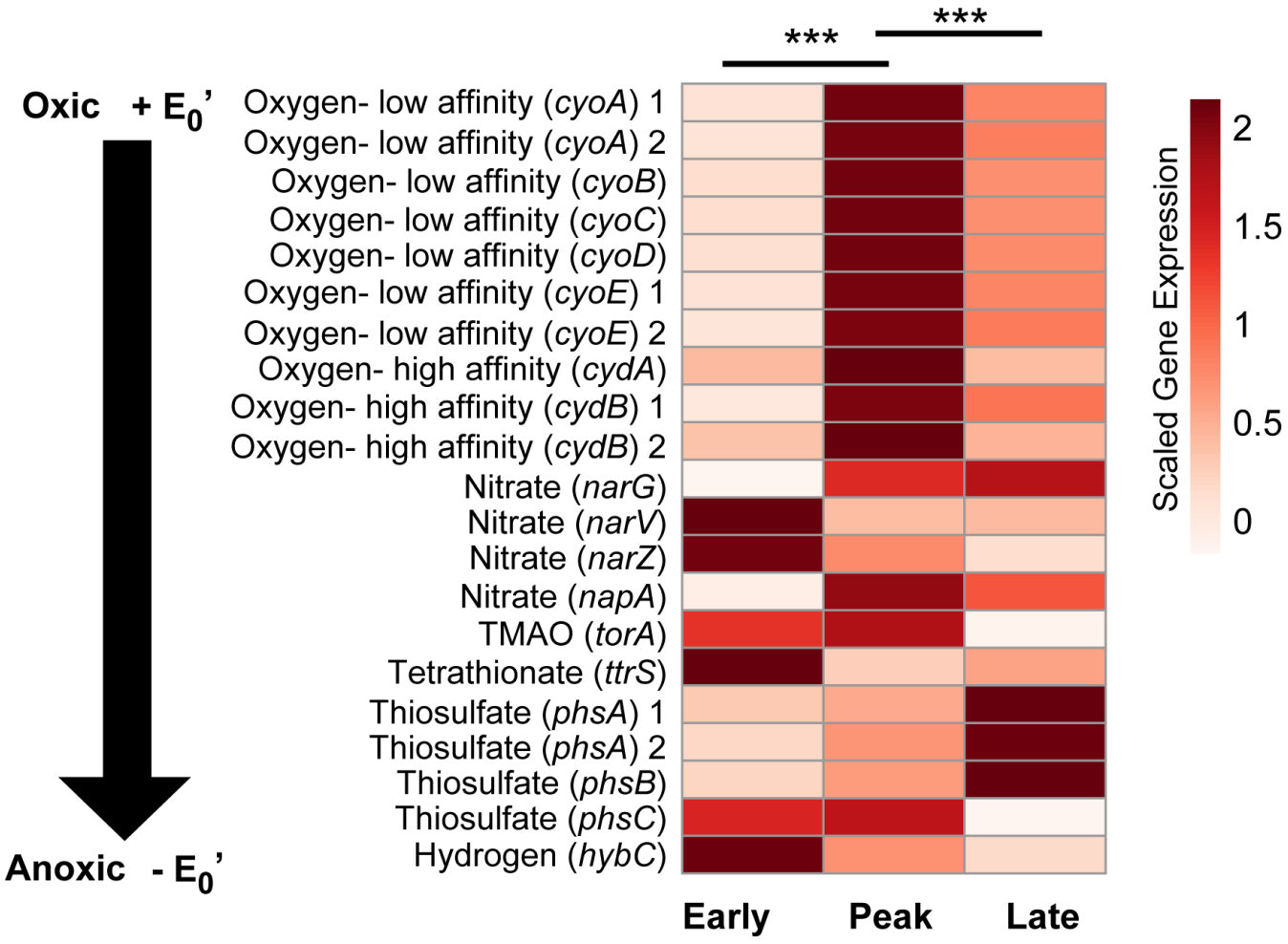

FIG 3 Respiratory electron acceptor utilization by infection phase in HFD-fed mice. Heatmap of the mean, normalized gene expression from respiratory electron acceptor utilization genes mapped to the *Salmonella* pangenome shows patterns between infection phases in HFD-fed mice. Genes are listed from oxic to anoxic (black arrow), and 15 samples are grouped by infection phase (early, peak, and late). Asterisks indicate statistical significance between phases where *** is a *P*-value of < 0.001.

expressed in the early- and late-infection phases. These data also demonstrate that multiple electron acceptor genes are activated simultaneously in the same infection phase, possibly reflecting subpopulation responses across the gut habitats (38, 50, 51) or co-metabolic regulatory control under common redox transcriptional regulators (52, 53), with the findings warranting further investigation. This dynamic gene expression highlights how an energetically versatile bacterium like *Salmonella* rapidly optimizes its energetic strategies to changing local chemical conditions during infection and as a consequence of host–pathogen–commensal microbiota interactions (23, 54–56).

Targeted and untargeted substrate profiles revealed during infection in HFD-fed mice

Prior studies have reported the multitude of electron donors that *Salmonella* can competitively utilize during respiration. In some cases, the pathogen utilizes lower-energy carbon substrates not viable for commensal obligate fermenters. Some of these include ethanolamine and 1,2-propanediol, which have been suggested to be important for *Salmonella* expansion over commensal microbes (18, 20, 22). Additionally, higher energy carbon sources, such as mannitol, arabinose, and galactitol, have been studied in relation to intracellular survival, *Salmonella* expansion, or competition (4, 6, 23, 57, 58).

While tracking the expression of genes that utilize these carbon sources throughout different infection phases in HFD-fed mice, we noticed significant expression changes for galactitol (*gatD*) during early infection. Notably, mannitol (*mtlA* and *mtlD*) and arabinose (*araA*, *araB*, and *araD*) were expressed across all infection phases and did not uniformly show enrichment over any infection phase. Additionally, ethanolamine (*eutC*) and 1,2-propanediol (*pduC*) were not discriminative of a particular infection phase but instead were predominately expressed during both the peak and late infection phases. In summary, our study design allowed us to track the gene expression of substrate use over time, adding new insights into *Salmonella* occupancy throughout infection in an HFD background.

Furthermore, our untargeted approach provided the potential to discover new putative substrates that may support *Salmonella* expansion, especially in this less-explored high-fat diet model. To do this, we examined the global clustering of substrate-related gene expression, comparing it with our metabolite data from HFD-infected, HFD-uninfected, and Chow-uninfected mice (Data Sets S3 and S4). The genes for utilizing carbon substrates clustered by infection phase (MRPP, $P = 0.002$) but not by mouse or timepoint (MRPP, $P > 0.05$) (Fig. 4A). Examining the differential expression of these carbon utilization genes across infection phases revealed distinct metabolic patterns. Early samples expressed a broader range of substrates, marked by differential expression of D-xylose isomerase (*xylA*). Supporting this, our metabolite data denoted decreases in xylose in the infected HFD samples (Fig. S4).

We also saw expression of carnitine utilization genes (*caiABCT*) (Fig. 4B), which were differentially expressed in late infection samples compared to peak infection samples. Carnitine has been shown to stimulate anerobic growth of *Salmonella,* which based on our respiration data occurs at the early and late infection phases (Fig. 3) (59, 60). Along with gene expression in late infection samples, we detected carnitine at day 7, the late phase of infection in HFD-infected mice (Fig. S4). Further research is needed to understand the impact of these metabolisms on *Salmonella* growth and physiology, as well as the interactions with the surrounding community.

Consistent with aerobic respiration being a hallmark of peak infection, we observed simultaneous differential expression of genes for utilizing isocitrate, succinate, and malate (*icdA*, *mdh*, *sdhABCD*, and *sucABCD*). It is possible that these genes were co-expressed with respiration due to roles in transforming intermediates of the tricarboxylic acid cycle, a critical component of aerobic respiration. However, it has also been shown that *Salmonella* can utilize microbially derived succinate as a substrate during aerobic respiration (21). In this study, the metabolite data showed less coordination with gene expression data, as succinate levels increased in the HFD-infected samples (Fig. S4). It is

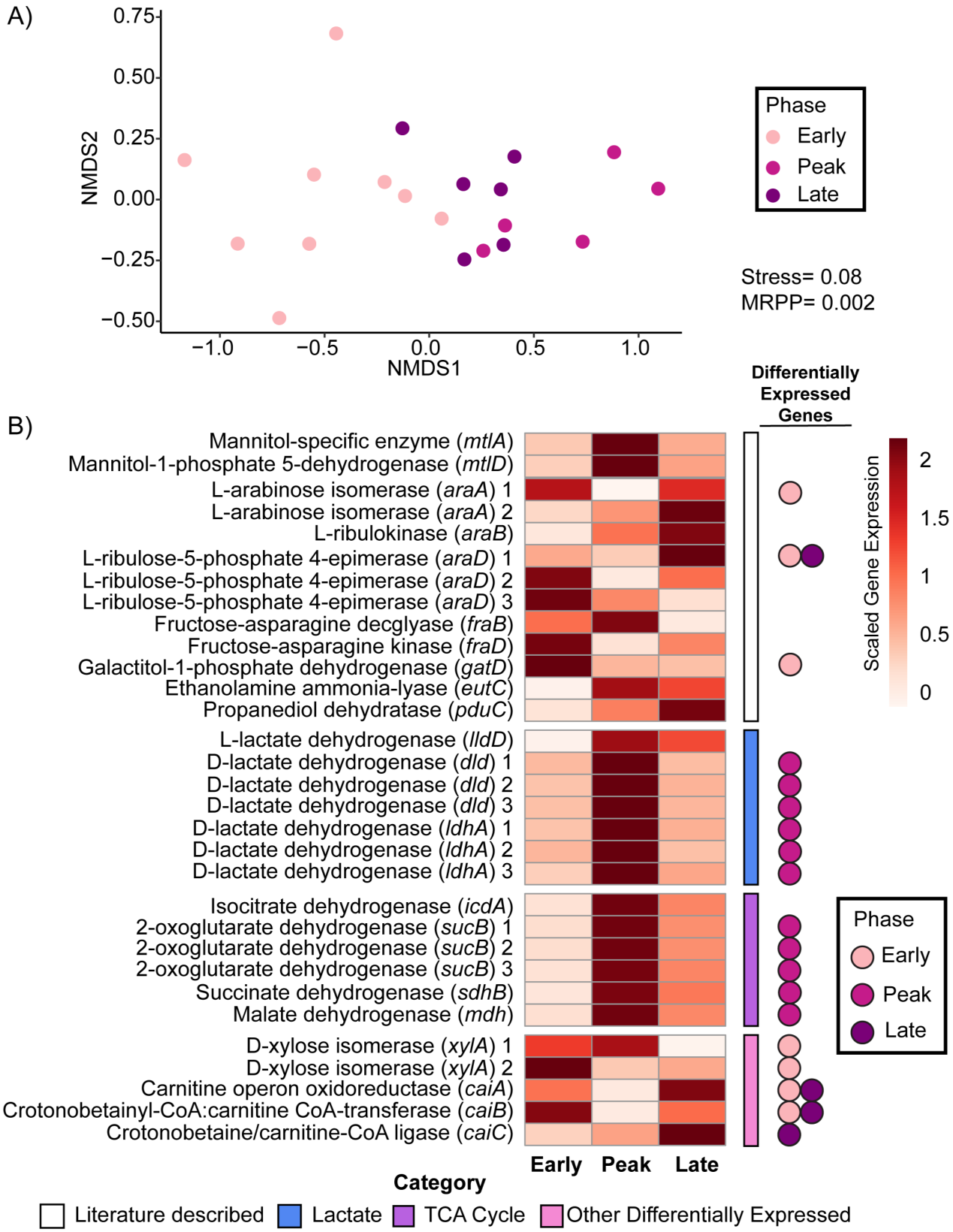

FIG 4 Differential expression of *Salmonella* carbon utilization genes by infection phase in HFD-fed mice. (A) Nonparametric multidimensional scaling (NMDS) depicts annotated *Salmonella* carbon utilization gene expression of samples from HFD-fed mice colored by infection phase (early: light pink, peak: dark pink, and late: purple). Bray–Curtis dissimilarity matrix from early, peak, and late samples (stress = 0.08) show significant grouping of *Salmonella* carbon utilization

(Continued on next page)

Fig 4 (Continued)

genes by infection phase (MRPP, $P = 0.002$) as found in Data Set S3. (B) Heatmap of the mean, normalized carbon utilization gene expression from our *Salmonella* pangenome shows patterns of carbon utilization by infection phase in HFD-fed mice. Genes were normalized across samples and via GeTMM normalization. Genes are grouped by carbon categories (literature described carbon: white; SCFA: blue; TCA cycle: purple; other differentially expressed carbon: bright pink). Genes that were characteristic of a specific phase (DESeq2 $P_{adj.} > 0.05$) are denoted on the side by colored circles (early: light pink, peak: dark pink, and late: purple) (Data Set S2).

possible that succinate was not used by *Salmonella* more than its microbial production or that the metabolite was additionally host-derived, as indicated in other studies on HFD mice (61). Unraveling the complex interactions of the host–microbiome–pathogen food web is warranted for this important gut metabolite (62).

Our targeted and untargeted transcriptomic approaches revealed the significance of lactate to overall *Salmonella* energy metabolism. Of the three lactate dehydrogenase genes in *Salmonella* (*ldhA*, *dld,* and *lldD*), the *ldhA* and *dld* genes encode an enzyme specific for the D-isomer of lactate, while the *lldD* gene encodes a protein with specificity for the L-isomer (19). It is thought that the host only produces the L-lactate isomer, while the microbial members can produce both isomers. Studies with gnotobiotic or microbiota-reduced mice have demonstrated the importance of L-lactate dehydrogenase (*lldD*) for *Salmonella* in utilizing host-derived lactate (19). Our targeted data show that the *lldD* gene was a core member of the transcriptome, detected across all timepoints but not distinguished by infection phase (Fig. S5A). However, our untargeted approach revealed that genes for utilizing D-lactate (*ldhA* and *dld*), likely derived from microbial production, were differentially expressed during peak infection when *Salmonella* was likely most rapidly growing based on respiration gene and ribosomal protein expression (Fig. 4B). Additionally, the metabolite data confirmed elevated levels of this compound at day 7 of infection relative to non-*Salmonella*-inoculated mice on either diet (Fig. S4), possibly indicating production exceeding consumption during the late phase of infection. This finding suggests new cross-feeding between the microbiome and *Salmonella*.

Non-nutritional gene expression patterns have implications on pathogenesis and horizontal gene transfer

Beyond nutritional requirements, we mined our data for other genes that were differentially expressed between phases and found categories of *Salmonella* pathogenesis genes that could be potential targets for therapeutic interventions. Volcano plots revealed gene expression patterns associated with differentially expressed genes between phases (early to peak/peak to late) with the following categories: (i) not significant (5,549/6,473), (ii) conjugation genes (22/NA), (iii) motility genes (9/28), (iv) outer membrane genes (33/13), (v) phage-like genes (22/4), (vi) other significant genes (940/141), and (vii) hypothetical genes (127/17) (Fig. 5; Data Set S2).

In early infection samples, we observed an upregulation of conjugation-, motility-, and fimbriae-related genes (Fig. 5A; Fig. S6). Conjugation facilitates the spread of virulence genes within *Salmonella* populations, influencing pathogen evolution (63). Additionally, motility and fimbriae genes support *Salmonella* movement and adhesion, which assist interactions with colonocytes and trigger the immune response (64–67). Notably, motility genes were also differentially expressed in the late phase compared to the peak phase. We consider it possible that *Salmonella* has enhanced chemotaxis to explore nutrient sources during the late infection phase or for environmental entry (68, 69).

The expression of many pathogenesis genes could not be discriminated by infection phase. For instance, type III secretion protein genes (*invAG*, *sptP*, *sspH12*, and *srfJ*) (Fig. S5; Data Set S2) were detected and highly expressed in all infection phases. Given their presumed role in initiation of infection and the inflammatory response, it was somewhat surprising that these genes were not discriminant of early expression but, instead, seemed active over the course of infection. We consider it possible that subpopulations

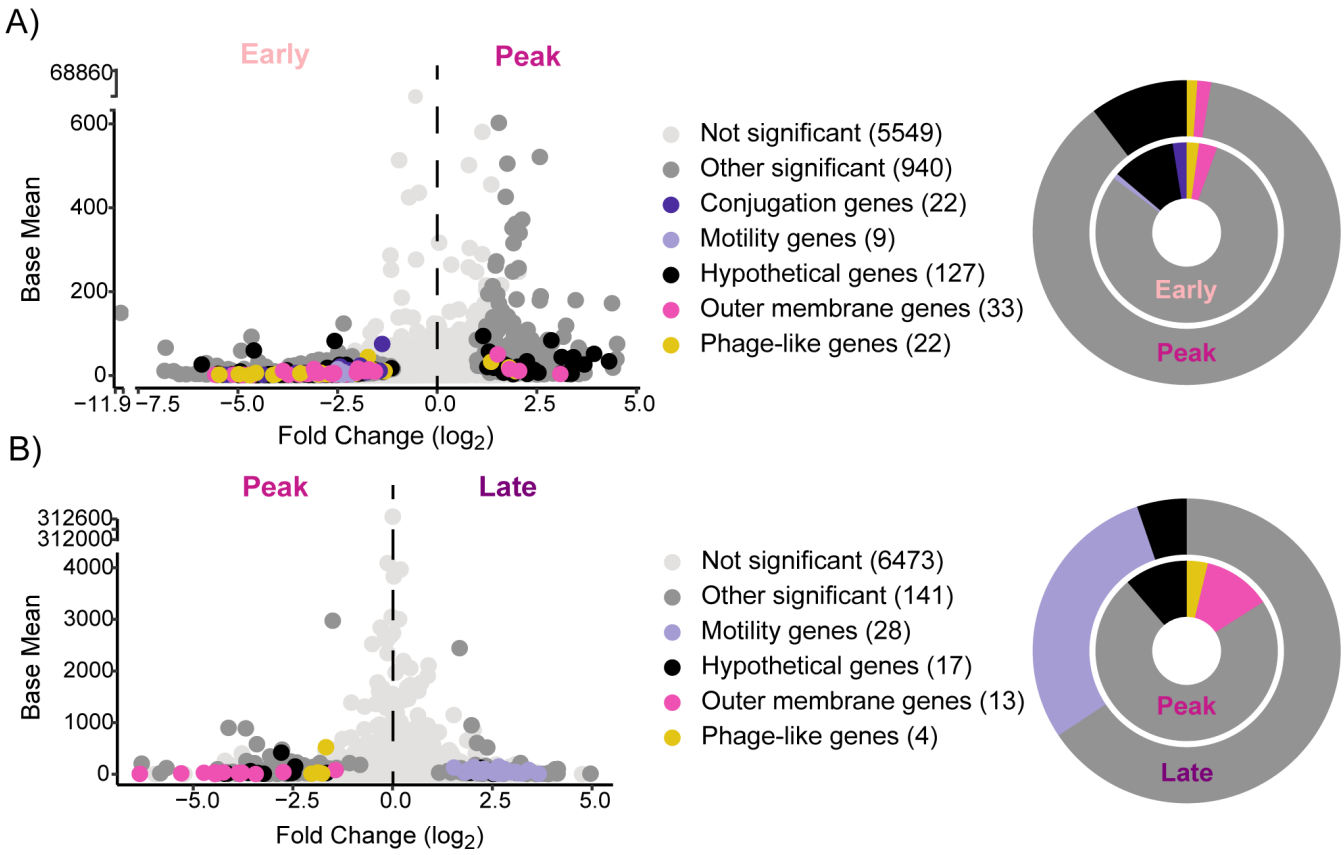

FIG 5 *Salmonella* pathogenesis gene expression between infection phases. Volcano plots (left) display differentially expressed genes between (A) early and peak or (B) peak and late infection samples. Each point represents a single gene, with point color indicating significance (DESeq2, $P_{adj.} > 0.05$) and annotation category. Numbers in parentheses next to each category indicate the number of genes in the *Salmonella* pangenome represented. Donut plots (right) highlight the proportion of significant genes within each category.

of *Salmonella* may be infecting host cells continually or inflammation-induced envelope stress might alter the expression of these genes, explaining their chronic expression (50, 70–72).

Comparatively, peak samples differentially expressed various outer membrane-associated genes (Fig. 5B; Fig. S7). Many of these genes were responsible for colanic acid synthesis (*wcaACDEFIJLM*). These genes protect bacteria from osmotic stress and are linked to biofilm formation (73–75). Additionally, cellulose synthase (*bcsA*), a sigma factor regulating genes controlling biofilm formation (*rpoS*), and a biofilm-dependent modulation protein were differentially expressed in the peak phase. Other biofilm-related genes (*adrA*, *csgACEFG*, *bcsBCE*, *mrlA*, and *ompR*) are highly expressed in the peak and late infection phases. This aligns with previous findings identifying *Salmonella* luminal biofilms, where nitrate mediates two *Salmonella* populations, resulting in virulent, planktonic cells and survival-adapted biofilm cells (76). Moreover, we detected differential expression of phage-like genes in both early and late infection. These prophage regions of the *Salmonella* genome carry virulence factors and are important for infection (49, 77, 78). Inflammation has been shown to boost prophage transfer between *Salmonella* species (79), but the role of phage in controlling *Salmonella* pathogenesis requires further investigation.

Conceptual model of *Salmonella* metabolism

In conclusion, this research contributes to the development of a conceptual model illustrating how the high-fat diet background impacts *Salmonella* gene expression (Fig. 6; Data Set S2). We show that *Salmonella* responds to a highly inflamed gut environment

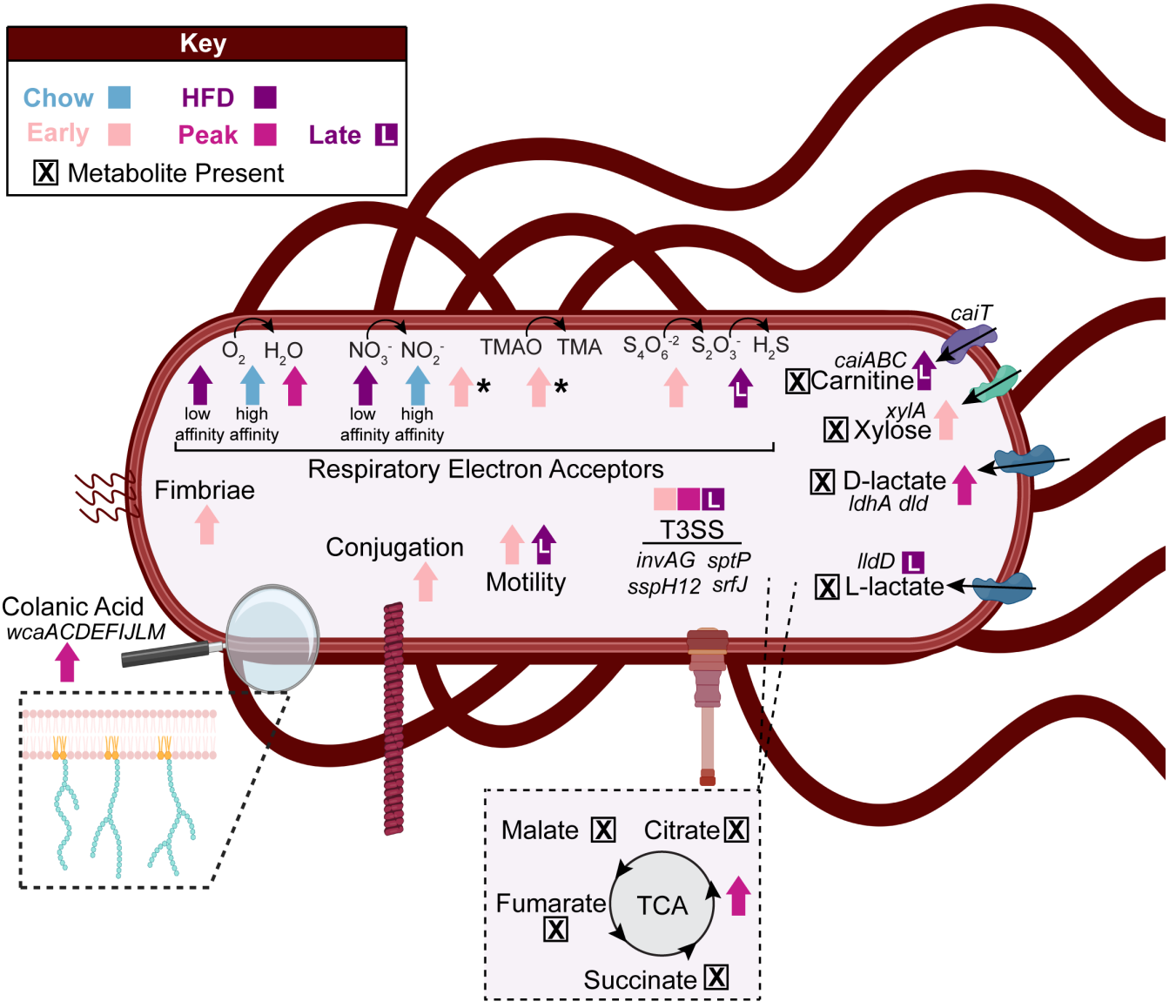

FIG 6 Conceptual model of findings across diet treatments and infection phases. The conceptual model summarizes our findings with regard to respiration, carbon utilization, other pathogenesis pathways, and nondifferentially expressed active genes. Arrows indicate the treatment (chow: blue, high-fat diet: purple) or infection phase (early: light pink, peak: dark pink, late: purple with the letter "L") with differential expression. The asterisk next to an arrow indicates differences between DESeq2 and GeTMM, where DESeq2 was prioritized for figure creation. Boxes with an "X" show metabolite presence (Data Sets S2 and S4).

and tactically uses respiratory electron acceptors and carbon sources over time. For example, our findings indicate differential isomer utilization of lactate, a critical gut SCFA (19). These findings highlight the potential microbial cross-feeding as well as affirm lactate utilization across infection phases, supporting the importance of this metabolite to *Salmonella*. When possible, we supported the gene expression data with metabolite data to provide additional insights into gut metabolite transformations (Fig. 6).

We also provide evidence for expression of genes related to pathogenesis, motility, and biofilms over the course of infection (Fig. 6). Surprisingly, virulence factor genes were not confined to the early stages when they are thought to function, but expressed across infection, indicating a heterogeneity in infection processes that were active even in a well-controlled, clonal experimental mouse model. Our discoveries benefitted from a well-established intellectual framework from years of detailed, curated pathogen physiological inquiry (11, 13, 80). This infrastructure provided a solid foundation that we

could both validate and build upon. Simultaneously, our work opens new avenues for research, offering fresh perspectives and opportunities for further exploration, including whether these trends persist in different regions of the gut or under other environmental conditions. For example, it would be warranted to compare the expression patterns from feces to those generated in the cecum in future studies. Moreover, this study offers a distinctive outlook on the early phases of *Salmonella* infection, providing gene expression data on days 1, 3, and 5 post-inoculation. These insights may enable research into curbing *Salmonella* proliferation during this critical period.

Conclusion

Despite being one of the most studied microbes, knowledge of *Salmonella* metabolism and pathogenesis in relevant diet contexts and across infection phases remains limited. In this study, we addressed this knowledge gap using a multi-omics approach, allowing us to examine existing theories (targeted approach) and develop new potential hypotheses (untargeted approach). In the targeted approach, we applied existing scientific knowledge to investigate specific genes previously implicated in *Salmonella* metabolism (4, 12, 13, 19–22), while the untargeted approach mines the data generated here for newly expressed functionalities discriminant of different infection phases. This work demonstrates the importance of time-dependent analysis in comprehending the finely tuned gene expression of *Salmonella* in response to the dynamic pathobiome environment.

This research lays the foundation for understanding how *Salmonella* pathogenesis and metabolism change under realistic dietary conditions within a dynamic gut ecosystem. Unraveling the intricacies of *Salmonella* metabolism can reveal key interaction junctures with the host and surrounding microbiota. The practical implications of this study may extend to the development of targeted therapeutics designed to disrupt specific pathogenic pathways or molecules, with the aim of minimizing adverse effects on host and microbiome functionalities.

MATERIALS AND METHODS

Strains and media

Salmonella enterica serovar Typhimurium strain 14028 was cultured at 37°C in Luria–Bertani (LB) broth overnight. This culture was washed and resuspended in water for inoculation.

Mouse experimentation and sample collection

Female CBA/J mice from The Jackson Laboratory (Bar Harbor, ME) were housed by treatment, with five mice per cage. Mice were fed either a fibrous chow diet (with 5.8% fat and 18.3% fiber, formula 7012, Teklad Diets) or a high-fat, no-fiber diet (with 36% fat and 0% fiber, formula F3282, Bio Serv) for 6 days before infection. Five HFD mice and 12 Chow mice were not inoculated with *Salmonella*, while the remaining mice (HFD = 5, Chow = 43) were inoculated with 10^9 CFUs of *S. enterica* Typhimurium strain 14028 via oral gavage on day 0 without treatment throughout the course of infection. Mice for multi-omics analysis were selected based on fecal sample availability. High responders among chow-fed, infected mice were chosen based on *Salmonella* reaching ≥25% relative abundance at any timepoint. Notably, unlike HFD mice, most Chow mice (n = 30) were not high responders. Animal experimentation was approved by IACUC (OSU 2009A0035). HFD mice were euthanized on day 8 due to severe disease represented by diarrhea, animal behavior, and animal lethargy, following IACUC protocols, while Chow mice were euthanized on day 16. Fecal samples were collected daily starting at diet transition until euthanization (except on days −5 and −4) on autoclaved aluminum

foil, transferred into labeled microcentrifuge tubes, and flash-frozen in liquid nitrogen. Samples were stored at −80°C until further processing.

DNA and RNA extraction and sequencing

Total nucleic acid was extracted using the Quick-DNA Fecal/Soil Microbe Miniprep Kit (Zymo Research) and stored at −20°C until amplicon sequencing could be performed. Amplicon sequencing was submitted to Argonne National Lab at the Next-Generation sequencing facility, using the Nextera XT DNA Library Preparation kit (Illumina) (data Set S1) and the Illumina MiSeq with 2 × 251 bp paired-end reads following HMP protocols (81). PCR amplification (30 cycles) of the V4 hypervariable region of the 16S rRNA gene was conducted with universal primers 515F and 806R, with the 515F primer containing a unique barcode.

RNA was extracted using the ZymoBIOMICS DNA/RNA Miniprep Kit (Zymo Research) and stored at −80°C until metatranscriptomic sequencing could be performed. RNA clean-up and library prep were performed using either the Ribo-Zero(TM) rRNA Removal Kit (Epicentre) with the Illumina Truseq Stranded RNA LT kit (Illumina) or Zymo-Seq RiboFree Total RNA Library Kit (Zymo Research) (Data Set S1). Chow samples were sequenced on the Illumina HiSeq2500 platform using 151-bp paired-end reads at the Genomics Shared Resource facility at the Ohio State University. High-fat diet samples were sequenced on the NovaSEQ6000 platform on an S4 flow cell using 151-bp paired-end reads at the University of Colorado-Anschutz Medical Campus at the Genomics Shared Resource Center.

16S rRNA amplicon sequencing analysis

Data were processed using Qiime2 2019.10 (82) with specific steps described here. In short, raw data fastq files were demultiplexed in Qiime2. Then, DADA2 was used for quality filtering, dereplication, denoising, removing chimeras, and merging sequences. Amplicon sequence variant (ASV) taxonomy was determined via SILVA release 132 SSU Ref NR 99 (83). Counts were filtered to ASVs with at least 10 reads in at least five samples. ASV feature table and taxonomic assignment are included (Data Set S1).

Long read sequencing and *Salmonella* pangenome generation

Genomic DNA for long read sequencing was extracted from our *Salmonella enterica* serovar Typhimurium strain 14028 isolate using the Quick-DNA Fecal/Soil Microbe Miniprep Kit (Zymo Research). Library preparation was performed using the Genomic DNA by Ligation (SQK-LSK 109) kit by Oxford Nanopore following the manufacturer's instructions and sequenced on the Flongle Flow Cell (R9.4.1) (Oxford Nanopore Technologies, Oxford, UK). Bases were called using Guppy (v 5.0.11), assembled using Flye (v2.8.3), and polished with long reads (84, 85). Our pangenome was created by concatenating called genes (DRAM [v1.4.0] [86]) from our highest-quality *Salmonella* short-read metagenome-assembled genome (33) and our best long-read *Salmonella*-assembled genome. After filtering duplicate genes at 99% minimum sequence identity using Mmseqs2 (Release 7-4e23d)(87), our *Salmonella* pangenome is 99.99% identical to the Joint Genome Institute *Salmonella* isolate. Genes were annotated using DRAM (v1.4.0)(86).

Metranscriptomics data analysis

Reads were quality-trimmed and had adapters removed using bbduk.sh (v38.89) (88) and mapped to our *Salmonella* pangenome using bowtie2 (v2.4.5) (89) using flags -D 10 R 2 N 0 L 22 -i S,0,2.50. Mapping files were filtered for high sequence identity (≥97%) using reformat.sh (88) and sorted by sequencing name using Samtools (v.1.9) (90). Counts were generated using htseq using flags -a 0 t CDS -i ID --stranded=reverse (v21.0.1) (91) and normalized using DESeq2 (92) or GeTMM (93) in R. For DESeq2 normalization, groups were based on infection phases (early, peak, and late). Infection phases were determined

by GeTMM normalized *Salmonella* S3 ribosomal protein (*rpsC*) expression. Samples were grouped into infection phases (early, peak, and late) based on the greatest increase in *Salmonella* S3 ribosomal protein per mouse, which is the peak sample for that mouse. Any samples before the peak S3 ribosomal protein expression were the early phase, whereas any samples after were the late phase. The five samples prior to *Salmonella* infection on day −1 were used as a control for nonspecific mapping.

Lipocalin-2 ELISA

Fecal samples were homogenized in PBS containing 0.1% Tween 20 (100 mg/mL) for 20 minutes, and then the resulting suspension was centrifuged at 12,000 rpm for 10 minutes at 4°C. The inflammation marker, lipocalin-2, was measured from the resulting supernatant using the Duoset murine Lcn-2 ELISA kit (R&D Systems, Minneapolis, MN). Measuring lipocalin-2 (Lcn-2) is a tractable, sensitive marker of host inflammation (35).

Metabolomics sequencing and analysis

For untargeted metabolomics, we used a 1 mL solution of three solvents (water/methanol/dichloromethane, 1/2/3, vol/vol/vol) to extract metabolites from fecal samples, disrupted with a sonicator (Bioruptor, Diagenode, Belgium). The resulting aqueous layer suspension was analyzed using Ultimate 300 liquid chromatography coupled to Thermo Q-Exactive plus mass spectrometer (Thermo Fisher Scientific, CA, USA) coupled to a mass spectrometer with two different separation columns (reverse-phase liquid chromatography and hydrophilic interaction liquid chromatography (HILIC)) for metabolome analysis. For reverse-phase separation, water with 0.1% (vol/vol) formic acid and acetonitrile with 0.1% (vol/vol) formic acid were used as mobile phases. The flow rate was set at 0.3 mL/min with the gradient as follows: 2% B for 0–2 minutes; 2%–30% B for 4 minutes; 30%–50% B for 8 minutes, 98% B for 1.5 minutes, and held at 98% B for 1 minute and then returning into initial gradient for equilibrium for 1.5 minutes. For HILIC separation, ACQUITY UPLC BEH HILIC 1.7 µm (2.1 × 150 mm) was used. Water/acetonitrile with 0.1% formic acid and 10 mM ammonium formate were prepared as solvent A (95/5, vol/vol) and solvent B (5/95, vol/vol). For gradient elution, 99% B was held for 2 minutes, gradually reduced to 75% B for 7 minutes, and reduced again to 45% B for 5 minutes. The gradient was held at 45% B for 2 minutes, returned to the initial gradient, and re-equilibrated for 5 minutes. The flow rate was set at 0.3 mL/min. The quality control (QC) sample was prepared for each sample and analyzed after every six samples. For data processing, peak-picking and metabolome annotation were processed with MS-Dial (v.4.90) (94).

For targeted metabolomics, the short-chain fatty acids were extracted as described previously and prepared using a previously published method (95). Briefly, 200 mM 3-NPH (3-nitrophenylhydrazine), 200 mM EDC (*N*-(3-dimethylaminopropyl)-*N*′-ethylcarbodiimide), and pyridine were added to extracted fecal SCFAs. Isotope-labeled SCFAs ($^{13}C_2$-acetic acid, $^{13}C_3$-propionic acid, and $^{13}C_4$-butyric acid) were added as an internal standard before derivatization. LC-MS/MS analysis of SCFAs was conducted using the ultimate 300 liquid chromatography and Thermo Quantiva Triple Quadrupole mass spectrometer (Thermo Fisher Scientific, CA, USA). Total run time for LC was 10 minutes with water with 0.1% of formic acid as mobile phase A and acetonitrile with 0.1% of formic acid as mobile phase B. The gradient started with 2% B, held for 0.5 minutes, linearly increased up to 98% B for 8 minutes, and re-equilibrated in 2% B for 1.5 minutes. Multiple concentrations of standard SCFAs (acetic acid, propionic acid, and butyric acid) were prepared alongside fecal SCFAs for quantitative analysis. The collected MS data were analyzed with Skyline (96).

Cecal CFU plates

To calculate the CFU of ceca of the HFD mice, one-third of the ceca was cut off and placed in 1 mL 1× sterile PBS in a pre-weighted tube. Ceca were then weighted and

homogenized under a tissue culture hood. One hundred microliters of the homogenization was placed in a 96-well plate and serially diluted to 10^{-7} (1:10 dilution steps). Ten microliters of each dilution from 0 to 10^{-5} was drop-plated on XLD media and incubated at 37°C for 16 hours and held in a cold room until counting.

Statistical analysis

Alpha diversity metrics, richness and Shannon's diversity, and significance values were calculated in R using the vegan package (v2.5-7) (97). To compare carbon utilization expression patterns among samples, Bray–Curtis dissimilarity was calculated using 406 *Salmonella* carbon utilization genes annotated by DRAM (Data Set S3). Annotation calls for CAZymes, central carbon, hydrocarbon, and pyruvate metabolism were selected as well as carbon-associated genes from our *Salmonella* DRAM module. Nonparametric multidimensional scaling (NMDS) plots were created using R (ggplot2 package v3.3.5 and the vegan package (v2.5-7) for visualization and nonparametric-fit quality was determined by stress value (97–99). Significance of infection phase carbon utilization expression differences was determined by analysis of similarity (ANOSIM) and multiple response permutation procedure (MRPP) (97). Heatmaps were generated with GeTMM normalize expression scaled by gene using the R package pheatmap (v1.0.12) (100).

ACKNOWLEDGMENTS

We acknowledge Erin Boulanger and Andrew Schwieters for their assistance with mouse experiments. We give special thanks to the integral work of Tyson Claffey and Richard Wolfe from the Colorado State University server management group, Sandy Shew for managing computing resources from The Ohio State University Unity cluster, and the Campus Chemical Instrument Center–Mass spectrometry & Proteomics at Ohio State University Comprehensive Cancer Center (OSU CCC) under the guidance of Dr. Pearlly Yan for supporting our use of metabolomics instruments.

This work was supported by NIH NIAID R01AI143288 awarded to V.H.W., B.M.M.A., and K.C.W.. Additional support came from NIH Predoctoral Training grants T32AI162691 (K.K.) and T32GM132057 (I.L.). The funders had no role in the study design, data collection, interpretation, or the decision to submit for publication. The microbial annotation tool, DRAM (86), received support from the DOE Office of Science, Office of Biological and Environmental Research (BER), grant no. DE-SC0021350.

A.S.-D., I.L., and M.S. conducted mouse experiments and collected fecal and cecal samples. R.K. and R.A.D. performed DNA and RNA extractions, ensuring quality control. K.K., Y.K., I.L., and M.S. analyzed and interpreted sequencing and metabolomic data. A.S.-D. quantified lipocalin-2 using ELISA. Y.K. and V.H.W. managed LC-MS/MS sample preparation and data collection for metabolomics. A.S.-D. and B.M.M.A. provided expertise on *Salmonella* physiology and experimentation. M.A.B. and K.C.W. provided guidance on microbial metabolism and sequencing best practices. K.K. and K.C.W. led the manuscript writing, with all co-authors contributing edits. The authors declare no competing interests.

AUTHOR AFFILIATIONS

[1]Department of Microbiology, Immunology, and Pathology, Colorado State University, Fort Collins, Colorado, USA
[2]Department of Microbial Infection and Immunity, The Ohio State University, Columbus, Ohio, USA
[3]Department of Chemistry and Biochemistry, The Ohio State University, Columbus, Ohio, USA
[4]Department of Cell and Molecular Biology, Colorado State University, Fort Collins, Colorado, USA

[5]Department of Soil and Crop Sciences, Colorado State University, Fort Collins, Colorado, USA

AUTHOR ORCIDs

Katherine Kokkinias http://orcid.org/0000-0002-1422-6372
Brian M. M. Ahmer http://orcid.org/0000-0002-4267-7322
Kelly C. Wrighton http://orcid.org/0000-0003-0434-4217

FUNDING

Funder	Grant(s)	Author(s)
HHS | NIH | National Institute of Allergy and Infectious Diseases (NIAID)	R01AI143288	Katherine Kokkinias Anice Sabag-Daigle Yongseok Kim Ikaia Leleiwi Michael Shaffer Richard Kevorkian Rebecca A. Daly Vicki H. Wysocki Mikayla A. Borton Brian M. M. Ahmer Kelly C. Wrighton
HHS | National Institutes of Health (NIH)	T32AI162691	Katherine Kokkinias
HHS | National Institutes of Health (NIH)	T32GM132057	Ikaia Leleiwi

AUTHOR CONTRIBUTIONS

Katherine Kokkinias, Conceptualization, Data curation, Formal analysis, Investigation, Methodology, Visualization, Writing – original draft, Writing – review and editing | Anice Sabag-Daigle, Data curation, Formal analysis, Investigation, Methodology, Writing – original draft, Writing – review and editing | Yongseok Kim, Data curation, Formal analysis, Investigation, Methodology, Writing – original draft, Writing – review and editing | Ikaia Leleiwi, Data curation, Formal analysis, Investigation, Methodology, Writing – review and editing | Michael Shaffer, Conceptualization, Data curation, Investigation, Methodology, Supervision, Writing – review and editing | Richard Kevorkian, Investigation, Writing – review and editing | Rebecca A. Daly, Data curation, Methodology, Project administration, Writing – original draft, Writing – review and editing | Vicki H. Wysocki, Conceptualization, Funding acquisition, Methodology, Writing – review and editing | Mikayla A. Borton, Conceptualization, Data curation, Methodology, Supervision, Validation, Writing – review and editing | Brian M. M. Ahmer, Conceptualization, Funding acquisition, Methodology, Writing – review and editing | Kelly C. Wrighton, Conceptualization, Funding acquisition, Methodology, Supervision, Validation, Visualization, Writing – original draft, Writing – review and editing

DATA AVAILABILITY

All data files and R scripts to generate figures are available in Github at https://github.com/Kokkinias/HFDtimeseries. All Salmonella MAGs and raw data are deposited at the National Center for Biotechnology Information (NCBI) under accession number PRJNA348350. The gene delineated Salmonella pangenome fasta file and pangenome annotation file, which are too large to be hosted in the supplemental data, are available in Zenodo at DOI 10.5281/zenodo.10479610.

ETHICS APPROVAL

Animal experimentation was approved by IACUC (OSU 2009A0035).

ADDITIONAL FILES

The following material is available online.

Supplemental Material

Data Set S1 (mSphere00534-24-s0001.xlsx). Metadata about the multi-omics performed, ASV feature count table, SILVA taxonomy (132-99-515-806), diversity metrics, lipocalin-2 concentrations,and HFD mouse weight.
Data Set S2 (mSphere00534-24-s0002.xlsx). Raw, unfiltered mapping to the *Salmonella* pangenome, gene length and strandedness information, GeTMM normalized gene counts, DESeq2 differentially expressed genes by each phase, DRAM (v1.4.0) annotations, and genes depicted in Fig. 6.
Data Set S3 (mSphere00534-24-s0003.xlsx). GeTMM normalized *Salmonella* carbon gene expression matrix, annotations of the *Salmonella* carbon gene from CAZyme and DRAM module step form, and the DRAM module step form (https://github.com/WrightonLabCSU/DRAM).
Data Set S4 (mSphere00534-24-s0004.xlsx). Abundance and annotations of untargeted metabolites and abundance of targeted short-chain fatty acids.
Supplemental Figures (mSphere00534-24-s0005.pdf). Figures S1 to S7.

REFERENCES

1. Majowicz SE, Musto J, Scallan E, Angulo FJ, Kirk M, O'Brien SJ, Jones TF, Fazil A, Hoekstra RM, International Collaboration on Enteric Disease "Burden of Illness" Studies. 2010. The global burden of nontyphoidal *Salmonella* gastroenteritis. Clin Infect Dis 50:882–889. https://doi.org/10.1086/650733
2. Centers for Disease Control and Prevention (CDC) Antibiotic Resistance Threats in the United States. 2013. Available from: https://www.cdc.gov/drugresistance/pdf/ar-threats-2013-508.pdf. Retrieved 26 Sep 2023.
3. Wotzka SY, Kreuzer M, Maier L, Arnoldini M, Nguyen BD, Brachmann AO, Berthold DL, Zünd M, Hausmann A, Bakkeren E, et al. 2019. *Escherichia coli* limits *Salmonella* Typhimurium infections after diet shifts and fat-mediated microbiota perturbation in mice. Nat Microbiol 4:2164–2174. https://doi.org/10.1038/s41564-019-0568-5
4. Eberl C, Weiss AS, Jochum LM, Durai Raj AC, Ring D, Hussain S, Herp S, Meng C, Kleigrewe K, Gigl M, Basic M, Stecher B. 2021. *E. coli* enhance colonization resistance against *Salmonella* Typhimurium by competing for galactitol, a context-dependent limiting carbon source. Cell Host Microbe 29:1680–1692. https://doi.org/10.1016/j.chom.2021.09.004
5. Litvak Y, Mon KKZ, Nguyen H, Chanthavixay G, Liou M, Velazquez EM, Kutter L, Alcantara MA, Byndloss MX, Tiffany CR, Walker GT, Faber F, Zhu Y, Bronner DN, Byndloss AJ, Tsolis RM, Zhou H, Bäumler AJ. 2019. Commensal *Enterobacteriaceae* protect against *Salmonella* colonization through oxygen competition. Cell Host Microbe 25:128–139. https://doi.org/10.1016/j.chom.2018.12.003
6. Prax N, Wagner S, Schardt J, Neuhaus K, Clavel T, Fuchs TM. 2021. A diet-specific microbiota drives *Salmonella* Typhimurium to adapt its *in vivo* response to plant-derived substrates. Anim Microbiome 3:24. https://doi.org/10.1186/s42523-021-00082-8
7. Jacobson A, Lam L, Rajendram M, Tamburini F, Honeycutt J, Pham T, Van Treuren W, Pruss K, Stabler SR, Lugo K, Bouley DM, Vilches-Moure JG, Smith M, Sonnenburg JL, Bhatt AS, Huang KC, Monack D. 2018. A gut commensal-produced metabolite mediates colonization resistance to *Salmonella* infection. Cell Host Microbe 24:296–307. https://doi.org/10.1016/j.chom.2018.07.002
8. Stecher B, Robbiani R, Walker AW, Westendorf AM, Barthel M, Kremer M, Chaffron S, Macpherson AJ, Buer J, Parkhill J, Dougan G, von Mering C, Hardt W-D. 2007. *Salmonella enterica* serovar Typhimurium exploits inflammation to compete with the intestinal microbiota. PLoS Biol 5:2177–2189. https://doi.org/10.1371/journal.pbio.0050244
9. Borton MA, Sabag-Daigle A, Wu J, Solden LM, O'Banion BS, Daly RA, Wolfe RA, Gonzalez JF, Wysocki VH, Ahmer BMM, Wrighton KC. 2017. Chemical and pathogen-induced inflammation disrupt the murine intestinal microbiome. Microbiome 5:47. https://doi.org/10.1186/s40168-017-0264-8
10. Rivera-Chávez F, Zhang LF, Faber F, Lopez CA, Byndloss MX, Olsan EE, Xu G, Velazquez EM, Lebrilla CB, Winter SE, Bäumler AJ. 2016. Depletion of butyrate-producing *Clostridia* from the gut microbiota drives an aerobic luminal expansion of *Salmonella*. Cell Host Microbe 19:443–454. https://doi.org/10.1016/j.chom.2016.03.004
11. Galán JE. 2021. *Salmonella* Typhimurium and inflammation: a pathogen-centric affair. Nat Rev Microbiol 19:716–725. https://doi.org/10.1038/s41579-021-00561-4
12. Winter SE, Thiennimitr P, Winter MG, Butler BP, Huseby DL, Crawford RW, Russell JM, Bevins CL, Adams LG, Tsolis RM, Roth JR, Bäumler AJ. 2010. Gut inflammation provides a respiratory electron acceptor for *Salmonella*. Nature 467:426–429. https://doi.org/10.1038/nature09415
13. Rogers AWL, Tsolis RM, Bäumler AJ. 2021. *Salmonella* versus the microbiome. Microbiol Mol Biol Rev. 85:e00027-19. https://doi.org/10.1128/MMBR.00027-19
14. Lopez CA, Rivera-Chávez F, Byndloss MX, Bäumler AJ. 2015. The periplasmic nitrate reductase NapABC supports luminal growth of *Salmonella enterica* serovar Typhimurium during colitis. Infect Immun 83:3470–3478. https://doi.org/10.1128/IAI.00351-15
15. Cruz E, Haeberle AL, Westerman TL, Durham ME, Suyemoto MM, Knodler LA, Elfenbein JR. 2023. Nonredundant dimethyl sulfoxide reductases influence *Salmonella enterica* serotype Typhimurium anaerobic growth and virulence. Infect Immun 91:e0057822. https://doi.org/10.1128/iai.00578-22
16. Kim KE, Chang GW. 1974. Trimethylamine oxide reduction by *Salmonella*. Can J Microbiol 20:1745–1748. https://doi.org/10.1139/m74-269
17. Nguyen BD, Cuenca V M, Hartl J, Gül E, Bauer R, Meile S, Rüthi J, Margot C, Heeb L, Besser F, Escriva PP, Fetz C, Furter M, Laganenka L, Keller P, Fuchs L, Christen M, Porwollik S, McClelland M, Vorholt JA, Sauer U, Sunagawa S, Christen B, Hardt W-D. 2020. Import of aspartate and malate by DcuABC drives H_2/fumarate respiration to promote initial

Salmonella gut-lumen colonization in mice. Cell Host Microbe 27:922–936. https://doi.org/10.1016/j.chom.2020.04.013
18. Price-Carter M, Tingey J, Bobik TA, Roth JR. 2001. The alternative electron acceptor tetrathionate supports B12-dependent anaerobic growth of *Salmonella enterica* serovar typhimurium on ethanolamine or 1,2-propanediol. J Bacteriol 183:2463–2475. https://doi.org/10.1128/JB.183.8.2463-2475.2001
19. Gillis CC, Hughes ER, Spiga L, Winter MG, Zhu W, Furtado de Carvalho T, Chanin RB, Behrendt CL, Hooper LV, Santos RL, Winter SE. 2018. Dysbiosis-associated change in host metabolism generates lactate to support *Salmonella* growth. Cell Host Microbe 23:54–64. https://doi.org/10.1016/j.chom.2017.11.006
20. Thiennimitr P, Winter SE, Winter MG, Xavier MN, Tolstikov V, Huseby DL, Sterzenbach T, Tsolis RM, Roth JR, Bäumler AJ. 2011. Intestinal inflammation allows *Salmonella* to use ethanolamine to compete with the microbiota. Proc Natl Acad Sci U S A 108:17480–17485. https://doi.org/10.1073/pnas.1107857108
21. Spiga L, Winter MG, Furtado de Carvalho T, Zhu W, Hughes ER, Gillis CC, Behrendt CL, Kim J, Chessa D, Andrews-Polymenis HL, Beiting DP, Santos RL, Hooper LV, Winter SE. 2017. An oxidative central metabolism enables *Salmonella* to utilize microbiota-derived succinate. Cell Host Microbe 22:291–301. https://doi.org/10.1016/j.chom.2017.07.018
22. Faber F, Thiennimitr P, Spiga L, Byndloss MX, Litvak Y, Lawhon S, Andrews-Polymenis HL, Winter SE, Bäumler AJ. 2017. Respiration of microbiota-derived 1,2-propanediol drives *Salmonella* expansion during colitis. PLoS Pathog 13:e1006129. https://doi.org/10.1371/journal.ppat.1006129
23. Steeb B, Claudi B, Burton NA, Tienz P, Schmidt A, Farhan H, Mazé A, Bumann D. 2013. Parallel exploitation of diverse host nutrients enhances *Salmonella* virulence. PLoS Pathog 9:e1003301. https://doi.org/10.1371/journal.ppat.1003301
24. Taylor SJ, Winter SE. 2020. *Salmonella* finds a way: metabolic versatility of *Salmonella enterica* serovar Typhimurium in diverse host environments. PLoS Pathog 16:e1008540. https://doi.org/10.1371/journal.ppat.1008540
25. Xiao L, Sonne SB, Feng Q, Chen N, Xia Z, Li X, Fang Z, Zhang D, Fjære E, Midtbø LK, et al. 2017. High-fat feeding rather than obesity drives taxonomical and functional changes in the gut microbiota in mice. Microbiome 5:43. https://doi.org/10.1186/s40168-017-0258-6
26. Daniel H, Gholami AM, Berry D, Desmarchelier C, Hahne H, Loh G, Mondot S, Lepage P, Rothballer M, Walker A, Böhm C, Wenning M, Wagner M, Blaut M, Schmitt-Kopplin P, Kuster B, Haller D, Clavel T. 2014. High-fat diet alters gut microbiota physiology in mice. ISME J 8:295–308. https://doi.org/10.1038/ismej.2013.155
27. Walker A, Pfitzner B, Neschen S, Kahle M, Harir M, Lucio M, Moritz F, Tziotis D, Witting M, Rothballer M, Engel M, Schmid M, Endesfelder D, Klingenspor M, Rattei T, Castell WZ, de Angelis MH, Hartmann A, Schmitt-Kopplin P. 2014. Distinct signatures of host–microbial meta-metabolome and gut microbiome in two C57BL/6 strains under high-fat diet. ISME J 8:2380–2396. https://doi.org/10.1038/ismej.2014.79
28. Kumar A, Henderson A, Forster GM, Goodyear AW, Weir TL, Leach JE, Dow SW, Ryan EP. 2012. Dietary rice bran promotes resistance to *Salmonella enterica* serovar Typhimurium colonization in mice. BMC Microbiol 12:71. https://doi.org/10.1186/1471-2180-12-71
29. Las Heras V, Clooney AG, Ryan FJ, Cabrera-Rubio R, Casey PG, Hueston CM, Pinheiro J, Rudkin JK, Melgar S, Cotter PD, Hill C, Gahan CGM. 2019. Short-term consumption of a high-fat diet increases host susceptibility to *Listeria monocytogenes* infection. Microbiome 7:7. https://doi.org/10.1186/s40168-019-0621-x
30. Gulhane M, Murray L, Lourie R, Tong H, Sheng YH, Wang R, Kang A, Schreiber V, Wong KY, Magor G, Denman S, Begun J, Florin TH, Perkins A, Cuív PÓ, McGuckin MA, Hasnain SZ. 2016. High fat diets induce colonic epithelial cell stress and inflammation that is reversed by IL-22. Sci Rep 6:28990. https://doi.org/10.1038/srep28990
31. Murakami Y, Tanabe S, Suzuki T. 2016. High-fat diet-induced intestinal hyperpermeability is associated with increased bile acids in the large intestine of mice. J Food Sci 81:H216–22. https://doi.org/10.1111/1750-3841.13166
32. Clemente-Suárez VJ, Beltrán-Velasco AI, Redondo-Flórez L, Martín-Rodríguez A, Tornero-Aguilera JF. 2023. Global impacts of western diet and its effects on metabolism and health: a narrative review. Nutrients 15:2749. https://doi.org/10.3390/nu15122749
33. Leleiwi I, Rodriguez-Ramos J, Shaffer M, Sabag-Daigle A, Kokkinias K, Flynn RM, Daly RA, Kop LFM, Solden LM, Ahmer BMM, Borton MA, Wrighton KC. 2023. Exposing new taxonomic variation with inflammation — a murine model-specific genome database for gut microbiome researchers. Microbiome 11:114. https://doi.org/10.1186/s40168-023-01529-7
34. Low A, Soh M, Miyake S, Aw VZJ, Feng J, Wong A, Seedorf H. 2021. Longitudinal changes in diet cause repeatable and largely reversible shifts in gut microbial communities of laboratory mice and are observed across segments of the entire intestinal tract. Int J Mol Sci 22:5981. https://doi.org/10.3390/ijms22115981
35. Chassaing B, Srinivasan G, Delgado MA, Young AN, Gewirtz AT, Vijay-Kumar M. 2012. Fecal lipocalin 2, a sensitive and broadly dynamic non-invasive biomarker for intestinal inflammation. PLoS ONE 7:e44328. https://doi.org/10.1371/journal.pone.0044328
36. Jarvik T, Smillie C, Groisman EA, Ochman H. 2010. Short-term signatures of evolutionary change in the *Salmonella enterica* serovar Typhimurium 14028 genome. J Bacteriol 192:560–567. https://doi.org/10.1128/JB.01233-09
37. Kushwaha SK, Bhavesh NLS, Abdella B, Lahiri C, Marathe SA. 2020. The phylogenomics of CRISPR-Cas system and revelation of its features in *Salmonella*. Sci Rep 10:21156. https://doi.org/10.1038/s41598-020-77890-6
38. Tsai CN, Coombes BK. 2019. The role of the host in driving phenotypic heterogeneity in *Salmonella*. Trends Microbiol 27:508–523. https://doi.org/10.1016/j.tim.2019.01.004
39. Hayden HS, Matamouros S, Hager KR, Brittnacher MJ, Rohmer L, Radey MC, Weiss EJ, Kim KB, Jacobs MA, Sims-Day EH, Yue M, Zaidi MB, Schifferli DM, Manning SD, Walson JL, Miller SI. 2016. Genomic analysis of *Salmonella enterica* serovar Typhimurium characterizes strain diversity for recent U.S. salmonellosis cases and identifies mutations linked to loss of fitness under nitrosative and oxidative stress. mBio 7:e00154. https://doi.org/10.1128/mBio.00154-16
40. Potter LC, Millington P, Griffiths L, Thomas GH, Cole JA. 1999. Competition between *Escherichia coli* strains expressing either a periplasmic or a membrane-bound nitrate reductase: does Nap confer a selective advantage during nitrate-limited growth? Biochem. J. 344 Pt 1:77–84. https://doi.org/10.1042/bj3440077
41. Gates AJ, Richardson DJ, Butt JN. 2008. Voltammetric characterization of the aerobic energy-dissipating nitrate reductase of *Paracoccus pantotrophus*: exploring the activity of a redox-balancing enzyme as a function of electrochemical potential. Biochem J 409:159–168. https://doi.org/10.1042/BJ20071088
42. Kranz RG, Barassi CA, Gennis RB. 1984. Immunological analysis of the heme proteins present in aerobically grown *Escherichia coli*. J Bacteriol 158:1191–1194. https://doi.org/10.1128/jb.158.3.1191-1194.1984
43. Rice CW, Hempfling WP. 1978. Oxygen-limited continuous culture and respiratory energy conservation in *Escherichia coli*. J Bacteriol 134:115–124. https://doi.org/10.1128/jb.134.1.115-124.1978
44. Jones-Carson J, Husain M, Liu L, Orlicky DJ, Vázquez-Torres A. 2016. Cytochrome *bd*-dependent bioenergetics and antinitrosative defenses in *Salmonella* pathogenesis. mBio 7:e02052-16. https://doi.org/10.1128/mBio.02052-16
45. He G, Shankar RA, Chzhan M, Samouilov A, Kuppusamy P, Zweier JL. 1999. Noninvasive measurement of anatomic structure and intraluminal oxygenation in the gastrointestinal tract of living mice with spatial and spectral EPR imaging. Proc Natl Acad Sci U S A 96:4586–4591. https://doi.org/10.1073/pnas.96.8.4586
46. Handa K, Ohmura M, Nishime C, Hishiki T, Nagahata Y, Kawai K, Suemizu H, Nakamura M, Wakui M, Kitagawa Y, Suematsu M, Tsukada K. 2010. Phosphorescence-assisted microvascular O_2 measurements reveal alterations of oxygen demand in human metastatic colon cancer in the liver of superimmunodeficient NOG mice, p 423–429. In Takahashi E, Bruley DF (ed), Oxygen transport to tissue XXXI. Springer US, Boston, MA.
47. Maier L, Vyas R, Cordova CD, Lindsay H, Schmidt TSB, Brugiroux S, Periaswamy B, Bauer R, Sturm A, Schreiber F, von Mering C, Robinson MD, Stecher B, Hardt W-D. 2013. Microbiota-derived hydrogen fuels

Salmonella Typhimurium invasion of the gut ecosystem. Cell Host Microbe 14:641–651. https://doi.org/10.1016/j.chom.2013.11.002
48. Shelton CD, Yoo W, Shealy NG, Torres TP, Zieba JK, Calcutt MW, Foegeding NJ, Kim D, Kim J, Ryu S, Byndloss MX. 2022. *Salmonella enterica* serovar Typhimurium uses anaerobic respiration to overcome propionate-mediated colonization resistance. Cell Rep 38:110180. https://doi.org/10.1016/j.celrep.2021.110180
49. Lopez CA, Winter SE, Rivera-Chávez F, Xavier MN, Poon V, Nuccio SP, Tsolis RM, Bäumler AJ. 2012. Phage-mediated acquisition of a type III secreted effector protein boosts growth of *Salmonella* by nitrate respiration. mBio 3:e00143-12. https://doi.org/10.1128/mBio.00143-12
50. Gebremichael Y, Crandall J, Mukhopadhyay R, Xu F. 2023. *Salmonella* subpopulations identified from human specimens express heterogenous phenotypes that are relevant to clinical diagnosis. Microbiol Spectr 11:e0167922. https://doi.org/10.1128/spectrum.01679-22
51. Liou MJ, Miller BM, Litvak Y, Nguyen H, Natwick DE, Savage HP, Rixon JA, Mahan SP, Hiyoshi H, Rogers AWL, Velazquez EM, Butler BP, Collins SR, McSorley SJ, Harshey RM, Byndloss MX, Simon SI, Bäumler AJ. 2022. Host cells subdivide nutrient niches into discrete biogeographical microhabitats for gut microbes. Cell Host Microbe 30:836–847. https://doi.org/10.1016/j.chom.2022.04.012
52. Teixidó L, Cortés P, Bigas A, Alvarez G, Barbé J, Campoy S. 2010. Control by Fur of the nitrate respiration regulators NarP and NarL in *Salmonella enterica*. Int Microbiol 13:33–39. https://doi.org/10.2436/20.1501.01.108
53. Cohen H, Adani B, Cohen E, Piscon B, Azriel S, Desai P, Bähre H, McClelland M, Rahav G, Gal-Mor O. 2022. The ancestral stringent response potentiator, DksA has been adapted throughout *Salmonella* evolution to orchestrate the expression of metabolic, motility, and virulence pathways. Gut Microbes 14:1997294. https://doi.org/10.1080/19490976.2021.1997294
54. Anderson CJ, Clark DE, Adli M, Kendall MM. 2015. Ethanolamine signaling promotes *Salmonella* niche recognition and adaptation during infection. PLoS Pathog 11:e1005278. https://doi.org/10.1371/journal.ppat.1005278
55. Gillis CC, Winter MG, Chanin RB, Zhu W, Spiga L, Winter SE. 2019. Host-derived metabolites modulate transcription of *Salmonella* genes involved in L-lactate utilization during gut colonization. Infect Immun 87:e00773-18. https://doi.org/10.1128/IAI.00773-18
56. Faber F, Tran L, Byndloss MX, Lopez CA, Velazquez EM, Kerrinnes T, Nuccio SP, Wangdi T, Fiehn O, Tsolis RM, Bäumler AJ. 2016. Host-mediated sugar oxidation promotes post-antibiotic pathogen expansion. Nature 534:697–699. https://doi.org/10.1038/nature18597
57. Wu J, Sabag-Daigle A, Borton MA, Kop LFM, Szkoda BE, Deatherage Kaiser BL, Lindemann SR, Renslow RS, Wei S, Nicora CD, Weitz KK, Kim Y-M, Adkins JN, Metz TO, Boyaka P, Gopalan V, Wrighton KC, Wysocki VH, Ahmer BMM. 2018. *Salmonella*-mediated inflammation eliminates competitors for fructose-asparagine in the gut. Infect Immun 86:e00945-17. https://doi.org/10.1128/IAI.00945-17
58. Ruddle SJ, Massis LM, Cutter AC, Monack DM. 2023. *Salmonella*-liberated dietary L-arabinose promotes expansion in superspreaders. Cell Host Microbe 31:405–417. https://doi.org/10.1016/j.chom.2023.01.017
59. Seim H, Löster H, Claus R, Kleber H-P, Strack E. 1982. Stimulation of the anaerobic growth of *Salmonella* Typhimurium by reduction of l-carnitine, carnitine derivatives and structure-related trimethylammonium compounds. Arch Microbiol 132:91–95. https://doi.org/10.1007/BF00690825
60. Koeth RA, Levison BS, Culley MK, Buffa JA, Wang Z, Gregory JC, Org E, Wu Y, Li L, Smith JD, Tang WHW, DiDonato JA, Lusis AJ, Hazen SL. 2014. γ-butyrobetaine is a proatherogenic intermediate in gut microbial metabolism of L-carnitine to TMAO. Cell Metab 20:799–812. https://doi.org/10.1016/j.cmet.2014.10.006
61. Li X, Huang G, Zhang Y, Ren Y, Zhang R, Zhu W, Yu K. 2023. Succinate signaling attenuates high-fat diet-induced metabolic disturbance and intestinal barrier dysfunction. Pharmacol Res 194:106865. https://doi.org/10.1016/j.phrs.2023.106865
62. Wei Y-H, Ma X, Zhao J-C, Wang X-Q, Gao C-Q. 2023. Succinate metabolism and its regulation of host-microbe interactions. Gut Microbes 15:2190300. https://doi.org/10.1080/19490976.2023.2190300
63. Ahmer BMM, Tran M, Heffron F. 1999. The virulence plasmid of *Salmonella typhimurium* is self-transmissible. J Bacteriol 181:1364–1368. https://doi.org/10.1128/JB.181.4.1364-1368.1999
64. Cogan TA, Jørgensen F, Lappin-Scott HM, Benson CE, Woodward MJ, Humphrey TJ. 2004. Flagella and curli fimbriae are important for the growth of *Salmonella enterica* serovars in hen eggs. Microbiology (Reading) 150:1063–1071. https://doi.org/10.1099/mic.0.26791-0
65. Tallant T, Deb A, Kar N, Lupica J, de Veer MJ, DiDonato JA. 2004. Flagellin acting via TLR5 is the major activator of key signaling pathways leading to NF-κB and proinflammatory gene program activation in intestinal epithelial cells. BMC Microbiol 4:33. https://doi.org/10.1186/1471-2180-4-33
66. Althouse C, Patterson S, Fedorka-Cray P, Isaacson RE. 2003. Type 1 fimbriae of *Salmonella enterica* serovar Typhimurium bind to enterocytes and contribute to colonization of swine *in vivo*. Infect Immun 71:6446–6452. https://doi.org/10.1128/IAI.71.11.6446-6452.2003
67. Stecher B, Hapfelmeier S, Müller C, Kremer M, Stallmach T, Hardt WD. 2004. Flagella and chemotaxis are required for efficient induction of *Salmonella enterica* serovar Typhimurium colitis in streptomycin-pretreated mice. Infect Immun 72:4138–4150. https://doi.org/10.1128/IAI.72.7.4138-4150.2004
68. Rivera-Chávez F, Winter SE, Lopez CA, Xavier MN, Winter MG, Nuccio SP, Russell JM, Laughlin RC, Lawhon SD, Sterzenbach T, Bevins CL, Tsolis RM, Harshey R, Adams LG, Bäumler AJ. 2013. *Salmonella* uses energy taxis to benefit from intestinal inflammation. PLoS Pathog 9:e1003267. https://doi.org/10.1371/journal.ppat.1003267
69. Stecher B, Barthel M, Schlumberger MC, Haberli L, Rabsch W, Kremer M, Hardt W-D. 2008. Motility allows *S. typhimurium* to benefit from the mucosal defence. Cell Microbiol 10:1166–1180. https://doi.org/10.1111/j.1462-5822.2008.01118.x
70. Palmer AD, Slauch JM. 2020. Envelope stress and regulation of the *Salmonella* pathogenicity island 1 type III secretion system. J Bacteriol 202:e00272-20. https://doi.org/10.1128/JB.00272-20
71. Ciolli Mattioli C, Eisner K, Rosenbaum A, Wang M, Rivalta A, Amir A, Golding I, Avraham R. 2023. Physiological stress drives the emergence of a *Salmonella* subpopulation through ribosomal RNA regulation. Curr Biol 33:4880–4892. https://doi.org/10.1016/j.cub.2023.09.064
72. Diard M, Hardt W-D. 2017. Basic processes in *Salmonella*-host interactions: within-host evolution and the transmission of the virulent genotype. Microbiol Spectr 5. https://doi.org/10.1128/microbiolspec.MTBP-0012-2016
73. Danese PN, Pratt LA, Kolter R. 2000. Exopolysaccharide production is required for development of *Escherichia coli* K-12 biofilm architecture. J Bacteriol 182:3593–3596. https://doi.org/10.1128/JB.182.12.3593-3596.2000
74. Prigent-Combaret C, Vidal O, Dorel C, Lejeune P. 1999. Abiotic surface sensing and biofilm-dependent regulation of gene expression in *Escherichia coli*. J Bacteriol 181:5993–6002. https://doi.org/10.1128/JB.181.19.5993-6002.1999
75. Navasa N, Rodríguez-Aparicio L, Martínez-Blanco H, Arcos M, Ferrero MA. 2009. Temperature has reciprocal effects on colanic acid and polysialic acid biosynthesis in *E. coli* K92. Appl Microbiol Biotechnol 82:721–729. https://doi.org/10.1007/s00253-008-1840-4
76. Miller AL, Nicastro LK, Bessho S, Grando K, White AP, Zhang Y, Queisser G, Buttaro BA, Tükel Ç. 2021. Nitrate is an environmental cue in the gut for *Salmonella enterica* serovar Typhimurium biofilm dispersal through curli repression and flagellum activation via cyclic-di-GMP signaling. mBio 13:e0288621. https://doi.org/10.1128/mbio.02886-21
77. Słomiński B, Całkiewicz J, Golec P, Węgrzyn G, Wróbel B. 2007. Plasmids derived from Gifsy-1/Gifsy-2, lambdoid prophages contributing to the virulence of *Salmonella enterica* serovar Typhimurium: implications for the evolution of replication initiation proteins of lambdoid phages and enterobacteria. Microbiology (Reading) 153:1884–1896. https://doi.org/10.1099/mic.0.2006/000802-0
78. Figueroa-Bossi N, Bossi L. 1999. Inducible prophages contribute to *Salmonella* virulence in mice. Mol Microbiol 33:167–176. https://doi.org/10.1046/j.1365-2958.1999.01461.x
79. Diard M, Bakkeren E, Cornuault JK, Moor K, Hausmann A, Sellin ME, Loverdo C, Aertsen A, Ackermann M, De Paepe M, Slack E, Hardt W-D.

2017. Inflammation boosts bacteriophage transfer between *Salmonella* spp. Science 355:1211–1215. https://doi.org/10.1126/science.aaf8451
80. Faber F, Bäumler AJ. 2014. The impact of intestinal inflammation on the nutritional environment of the gut microbiota. Immunol Lett 162:48–53. https://doi.org/10.1016/j.imlet.2014.04.014
81. Caporaso JG, Lauber CL, Walters WA, Berg-Lyons D, Lozupone CA, Turnbaugh PJ, Fierer N, Knight R. 2011. Global patterns of 16S rRNA diversity at a depth of millions of sequences per sample. Proc Natl Acad Sci U S A 108 Suppl 1:4516–4522. https://doi.org/10.1073/pnas.1000080107
82. Bolyen E, Rideout JR, Dillon MR, Bokulich NA, Abnet CC, Al-Ghalith GA, Alexander H, Alm EJ, Arumugam M, Asnicar F, et al. 2019. Reproducible, interactive, scalable and extensible microbiome data science using QIIME 2. Nat Biotechnol 37:852–857. https://doi.org/10.1038/s41587-019-0209-9
83. Quast C, Pruesse E, Yilmaz P, Gerken J, Schweer T, Yarza P, Peplies J, Glöckner FO. 2013. The SILVA ribosomal RNA gene database project: improved data processing and web-based tools. Nucleic Acids Res 41:D590–D596. https://doi.org/10.1093/nar/gks1219
84. Wick RR, Judd LM, Holt KE. 2019. Performance of neural network basecalling tools for Oxford Nanopore sequencing. Genome Biol 20:129. https://doi.org/10.1186/s13059-019-1727-y
85. Kolmogorov M, Yuan J, Lin Y, Pevzner PA. 2019. Assembly of long, error-prone reads using repeat graphs. Nat Biotechnol 37:540–546. https://doi.org/10.1038/s41587-019-0072-8
86. Shaffer M, Borton MA, McGivern BB, Zayed AA, La Rosa SL, Solden LM, Liu P, Narrowe AB, Rodríguez-Ramos J, Bolduc B, Gazitúa MC, Daly RA, Smith GJ, Vik DR, Pope PB, Sullivan MB, Roux S, Wrighton KC. 2020. DRAM for distilling microbial metabolism to automate the curation of microbiome function. Nucleic Acids Res 48:8883–8900. https://doi.org/10.1093/nar/gkaa621
87. Steinegger M, Söding J. 2017. MMseqs2 enables sensitive protein sequence searching for the analysis of massive data sets. Nat Biotechnol 35:1026–1028. https://doi.org/10.1038/nbt.3988
88. Bushnell B. 2014. BBMap: a fast, accurate, splice-aware aligner. Available from: https://sourceforge.net/projects/bbmap
89. Langmead B, Salzberg SL. 2012. Fast gapped-read alignment with Bowtie 2. Nat Methods 9:357–359. https://doi.org/10.1038/nmeth.1923
90. Danecek P, Bonfield JK, Liddle J, Marshall J, Ohan V, Pollard MO, Whitwham A, Keane T, McCarthy SA, Davies RM, Li H. 2021. Twelve years of SAMtools and BCFtools. Gigascience 10:giab008. https://doi.org/10.1093/gigascience/giab008
91. Anders S, Pyl PT, Huber W. 2015. HTSeq—a Python framework to work with high-throughput sequencing data. Bioinformatics 31:166–169. https://doi.org/10.1093/bioinformatics/btu638
92. Love MI, Huber W, Anders S. 2014. Moderated estimation of fold change and dispersion for RNA-seq data with DESeq2. Genome Biol 15:550. https://doi.org/10.1186/s13059-014-0550-8
93. Smid M, Coebergh van den Braak RRJ, van de Werken HJG, van Riet J, van Galen A, de Weerd V, van der Vlugt-Daane M, Bril SI, Lalmahomed ZS, Kloosterman WP, Wilting SM, Foekens JA, IJzermans JNM, Martens JWM, Sieuwerts AM, MATCH study group. 2018. Gene length corrected trimmed mean of M-values (GeTMM) processing of RNA-seq data performs similarly in intersample analyses while improving intrasample comparisons. BMC Bioinformatics 19:236. https://doi.org/10.1186/s12859-018-2246-7
94. Tsugawa H, Ikeda K, Takahashi M, Satoh A, Mori Y, Uchino H, Okahashi N, Yamada Y, Tada I, Bonini P, Higashi Y, Okazaki Y, Zhou Z, Zhu Z-J, Koelmel J, Cajka T, Fiehn O, Saito K, Arita M, Arita M. 2020. A lipidome atlas in MS-DIAL 4. Nat Biotechnol 38:1159–1163. https://doi.org/10.1038/s41587-020-0531-2
95. Han J, Lin K, Sequeira C, Borchers CH. 2015. An isotope-labeled chemical derivatization method for the quantitation of short-chain fatty acids in human feces by liquid chromatography–tandem mass spectrometry. Anal Chim Acta 854:86–94. https://doi.org/10.1016/j.aca.2014.11.015
96. Adams KJ, Pratt B, Bose N, Dubois LG, St John-Williams L, Perrott KM, Ky K, Kapahi P, Sharma V, MacCoss MJ, Moseley MA, Colton CA, MacLean BX, Schilling B, Thompson JW, Alzheimer's Disease Metabolomics Consortium. 2020. Skyline for small molecules: a unifying software package for quantitative metabolomics. J Proteome Res 19:1447–1458. https://doi.org/10.1021/acs.jproteome.9b00640
97. OksanenJ, SimpsonG, Blanchet F, Kindt R, Legendre P, Minchin P, O'HaraR, Solymos P, Stevens M, Szoecs E. 2022. _vegan: community ecology package_. R package version 2.6-4. https://CRAN.R-project.org/package=vegan.
98. Clarke KR. 1993. Non-parametric multivariate analyses of changes in community structure. Aust J Ecol18:117–143. https://doi.org/10.1111/j.1442-9993.1993.tb00438.x
99. Wickham H. 2016. *Ggplot2: elegant graphics for data analysis (3e)*. Springer-Verlag New York. https://ggplot2-book.org/.
100. KoldeR. 2019. Pheatmap: pretty heatmaps (1.0.12). Available from: https://CRAN.R-project.org/package=pheatmap